

Distributions of Envelope and Phase in Wind Waves

M. AZIZ TAYFUN

College of Engineering & Petroleum, Kuwait University, Safat, Kuwait

(Manuscript received 12 March 2008, in final form 23 May 2008)

ABSTRACT

A theoretical expression derived previously for describing the joint distribution of the envelope and phase of second-order nonlinear waves is verified with wind wave measurements gathered in the North Sea. The same distribution is explored further to obtain the marginal and conditional distributions of wave envelopes and phases. The nature and implications of these are examined, with emphasis on the occurrence of large waves and associated phases. It is shown that the wave phase distribution assumes two distinct forms depending on whether envelope heights exceed the significant envelope height. For envelope heights sufficiently larger than this threshold, the wave phase distribution approaches a simple limit form, indicating that large surface displacements can occur only above the mean sea level. Comparisons with the North Sea data confirm these theoretical results and indicate that large surface displacements and thus large waves result from the random superposition of elementary spectral components enhanced by second-order nonlinear interactions. Further, large waves with higher and sharper crests do not display any secondary maxima or minima. They appear more regular or “narrow banded” than relatively low waves, and their heights and crests do not violate the Miche–Stokes-type upper limits. The results also suggest that third-order nonlinearities do not affect the surface statistics in any discernable way.

1. Introduction

The surface displacement from the mean sea level observed at a fixed point in time t admits a general representation of the form $\eta(t) = \xi \cos \phi$, where $\xi(t)$ and $\phi(t)$ represent the wave envelope and wave phase, respectively. These definitions are valid for linear and nonlinear waves in general. In linear waves, η is Gaussian and the probability density (PD) describing ξ and ϕ jointly assumes the well-known form (Longuet-Higgins 1957)

$$p_{\phi\xi} = p_{\phi}p_{\xi} = (1/2\pi)\xi \exp(-\xi^2/2), \quad (1)$$

where it is assumed that all elevations are scaled with the root-mean-square σ of η . Thus, ξ and ϕ are statistically independent, ϕ by itself is uniformly random, say in $(-\pi, \pi)$, and ξ is Rayleigh distributed. Several theoretical results of practical value including, most notably, the approximate form of the joint distribution of zero-crossing amplitudes and periods in narrowband

seas follows from a more generalized form of Eq. (1) describing the joint distribution of ξ , ϕ , and first-order derivatives (Longuet-Higgins 1957, 1975; Goda 1978).

In second-order nonlinear waves, η is non-Gaussian, and the joint PD of ξ and ϕ is modified as (Tayfun 1994)

$$p_{\phi\xi} = p_{\phi|\xi}p_{\xi}, \\ = \frac{1}{2\pi} \left[1 + \frac{\lambda_3}{6} \xi(\xi^2 - 4) \cos \phi \right] \xi \exp(-\xi^2/2), \quad (2)$$

where $\lambda_3 = \langle \eta^3 \rangle$ and the angle brackets denote a statistical average. This result, valid for directional waves in deep and shallower water depths, agrees with earlier approximations derived under less general conditions (Tayfun and Lo 1989, 1990; Tayfun 1990). It also suggests a somewhat more complex structure in which ϕ and ξ are no longer statistically independent since $p_{\phi\xi} \neq p_{\phi}p_{\xi}$.

The derivation of Eq. (2), which requires a bivariate Gram–Charlier series expansion of the joint statistics of η and its Hilbert transform $\hat{\eta} = \xi \sin \phi$, is elaborated elsewhere and thus not repeated here (Tayfun 1994; see also Tayfun and Lo 1990). A generalization to include the first-order derivatives of ξ and ϕ in the joint

Corresponding author address: M. Aziz Tayfun, College of Engineering & Petroleum, Kuwait University, P.O. Box 5969, Safat 13060, Kuwait.
E-mail: aziztayfun@usa.net

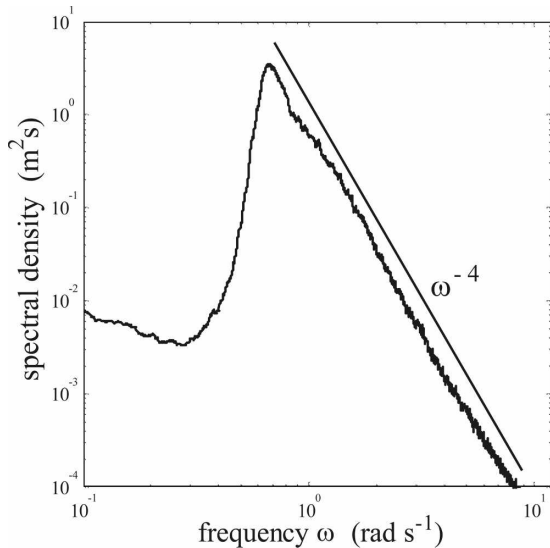


FIG. 1. WACSIS: spectral density of surface displacements.

statistics has not thus far been considered, nor is it contemplated in this paper as it requires a cumbersome four-variate Gram–Charlier series expansion of the joint statistics of η , $\hat{\eta}$, and associated first-order derivatives.

Tayfun and Lo (1989, 1990) and Tayfun (1994) explored the marginal distributions describing ξ and ϕ by themselves and compared these to oceanic data and simulations representative of deep water waves. The oceanic data comprised a series of one-hourly measurements gathered at a relatively poor sampling rate of 1 Hz in the Gulf of Mexico during the passage of Hurricane Camille in 1969. The results indicated that the second-order theoretical expressions describe the observed distributions reasonably well, especially when nonlinear effects are sufficiently pronounced and the duration of measurements is of the order of several hours. More recently, Rodriguez et al. (1998) and Cherneva and Guedes Soares (2006) carried out further comparisons, albeit only with wave phases. In particular, Rodriguez et al. (1998) examined several wave phase histograms, each extracted from a single 20-min time series gathered by a wave buoy. The nature of these histograms appears contradictory to the theoretical expectations in all cases, irrespective of whether the observations represented nearly linear or nonlinear waves. In contrast, the results of Cherneva and Guedes Soares (2006) derived from somewhat longer series suggest that the theoretical wave phase distribution describes the observed data well except in shallower water depths where waves exhibit rather pronounced nonlinear characteristics, plausibly due to shoaling and higher-order nonlinear effects.

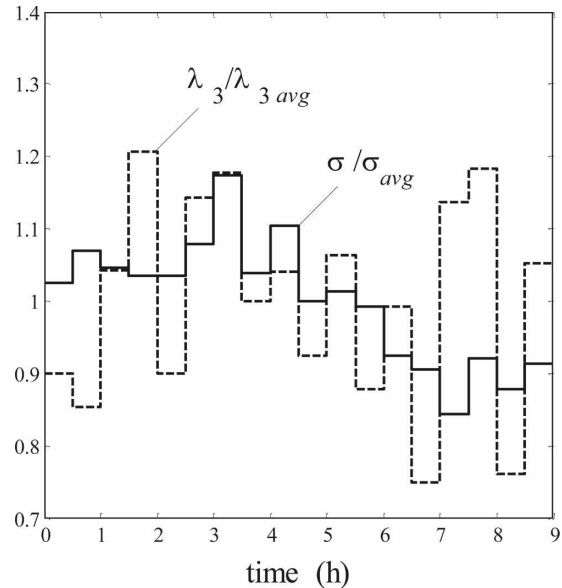


FIG. 2. WACSIS: half-hourly variations of σ and λ_3 ($\sigma_{avg} = 0.981$, $\lambda_{3avg} = 0.231$).

This study elaborates Eq. (2) further and compares it with more recent measurements gathered at a relatively shallow water depth in the North Sea. The same expression is then used to obtain a variety of theoretical expressions describing the conditional distributions of ξ and ϕ , with emphasis on large surface displacements, large waves, and the nature of associated phases. Some limited comparisons similar to those in the aforementioned studies are also given as further verification of theoretical results. Subsequently, and mostly because of the current interest in exceptionally large waves, the validity of Miche–Stokes-type upper bounds to large wave heights and crests, and the possible effects of third-order nonlinear corrections on the associated statistics are also examined to some extent.

2. North Sea data

The wind wave data that will be used for verifying theoretical results comprise 9-h measurements gathered at 4 Hz with a Baylor wave staff from the Meetpost Noordwijk platform in 18-m average water depth in the southern North Sea in January 1998 as part of the Wave Crest Sensor Intercomparison Study (Forristall et al. 2002). This data, hereafter referred to as WACSIS, represents fairly energetic waves. Figure 1 suggests that the spectral density of surface displacements tends to a ω^{-4} power law over frequencies slightly larger than the spectral peak frequency $\omega_p \cong 0.665$ rad s $^{-1}$. Figure 2

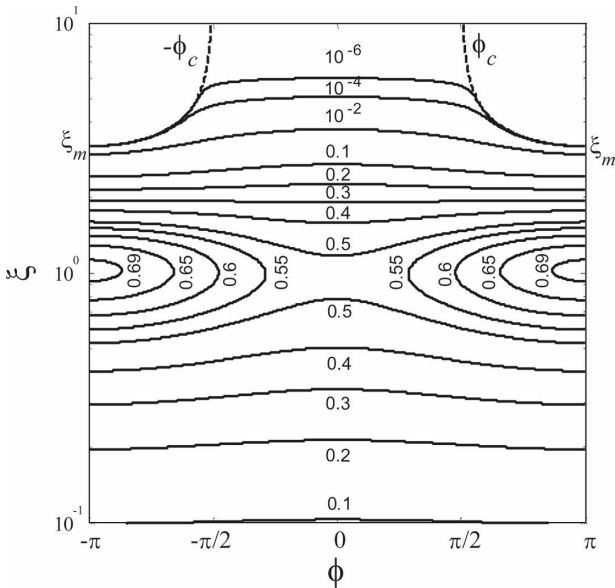


FIG. 3. Contours of $2\pi p_{\phi\xi} = \text{const}$ from Eq. (2) and boundary curves $\pm\phi_c$ of Eq. (3) for $\lambda_3 = 0.3$.

shows the variations of σ and λ_3 estimated from half-hourly segments. The segmental σ estimates differ from the overall average $\sigma_{\text{avg}} = 0.981$ m by as much as $\pm 17\%$; $\lambda_{3\text{avg}} = 0.231$ as an overall average, but the half-hourly samples vary from 0.172 to 0.278. These represent fairly significant nonstationary and nonlinear characteristics. To compensate for nonstationarity at least partially, all analyses will be based on half-hourly segments, scaling the surface displacements in each segment with the corresponding σ estimate.

3. Joint distribution of wave envelope and phase

For $\lambda_3 = 0.3$ as a hypothetical case, Fig. 3 shows various contours of $2\pi p_{\phi\xi}$ derived from Eq. (2). These noticeably differ from similar contours of $2\pi p_{\phi\xi}$ in linear waves since the latter would appear as straight parallel lines if plotted in the same figure. Also note that $p_{\phi\xi} < 0$ in $\Omega \equiv \{\phi_c < |\phi| \leq \pi, \xi > \xi_m\}$, where

$$\phi_c = \cos^{-1}[-6/\lambda_3\xi(\xi^2 - 4)]; \quad \xi > \xi_m, \quad (3)$$

and ξ_m is such that

$$1 - \frac{\lambda_3}{6} \xi_m(\xi_m^2 - 4) = 0. \quad (4)$$

In general, $\xi_m > 2$ and readily follows by iteration from $\xi_{m,j+1} = [(6/\lambda_3) + 4\lambda_{m,j}]^{1/3}$, with $j = 0, 1, 2, \dots$ and $\xi_{m,0} = 2$. Clearly, the values of ϕ and ξ in Ω lie above the curves $\pm\phi_c$. Oceanic values of λ_3 are typically less than 0.3. Nonetheless, numerical computations for

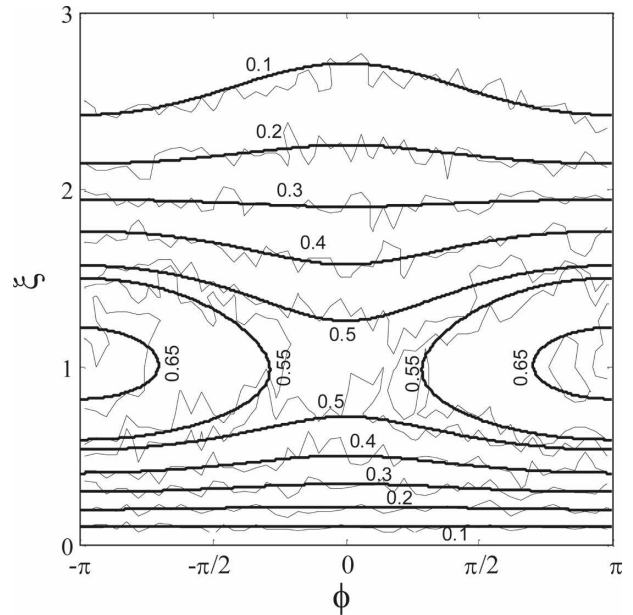


FIG. 4. Contours of $2\pi p_{\phi\xi} = \text{const}$: WACSIS data compared to predictions from Eq. (2).

$0.05 \leq \lambda_3 \leq 0.5$ indicate that the probability mass over Ω is less than 10^{-3} in absolute value. So, no adjustment is really necessary in Eq. (2) for practical applications. The nonnegativity requirement will have more relevance later in considering the conditional PD of ϕ , given ξ , whenever $\xi > \xi_m$.

Figure 4 compares WACSIS with the theoretical contours $2\pi p_{\phi\xi} = 0.1, 0.2, \dots$ from Eq. (2). It appears that the theoretical expression represents the observed data reasonably well. The boundary curves $\pm\phi_c$, the scatter of wave phases and associated envelopes derived from half-hourly segments of WACSIS are shown in Fig. 5 for $\xi > 2$. The theoretical curves $\pm\phi_c$ are for $\lambda_{3\text{avg}} = 0.231$, the overall average of 18 half-hourly segments. It is observed that if $\xi > \xi_m$, the physically realizable values of ϕ tend to lie in $(-\phi_c, \phi_c)$. Further, $\phi_c \rightarrow \pi/2$ for $\xi \gg 1$, in which case $\eta > 0$ necessarily. So, relatively large surface displacements are likely only above the mean sea level. In linear waves, surface displacements no matter how large are equally likely both above and below the mean level.

Figure 5 also indicates the envelopes and phases associated with the two largest surface displacements, η_1 and η_2 . The corresponding wave heights, envelopes, phases, and conjugates are $h_1 = 9.270$, $\xi_1 = 6.042$, $\phi_1 = -0.028$, and $\hat{\eta}_1 = -0.171$ for $\eta_1 = 6.039$; and $h_2 = 7.955$, $\xi_2 = 5.050$, $\phi_2 = 0.347$, and $\hat{\eta}_2 = 1.715$ for $\eta_2 = 4.749$. The largest four envelope heights in the figure congregate around η_1 , the crest of the largest wave. In general, large surface displacements do not occur simulta-

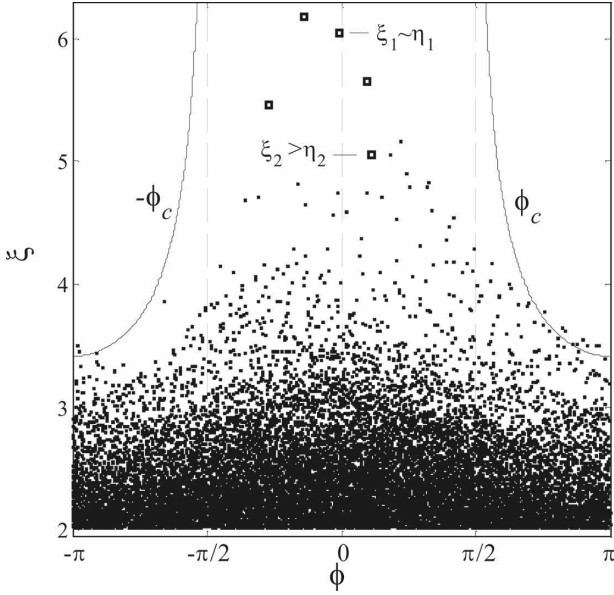


FIG. 5. WACSIS: the scatter diagram of ϕ and $\xi > 2$, boundary curves $\pm\phi_c$ of Eq. (3), envelopes (ξ_1 and ξ_2), and phases associated with two largest waves and their crests (η_1 and η_2).

neously with largest envelope heights, but they would do so if the associated phases also approach zero simultaneously, as for ξ_1 and η_1 . The latter condition implies the random superposition of a sufficiently large number of wave components as their phases tend to zero simultaneously. In wind waves, linear or otherwise, this is the most likely process that generates large surface displacements and unusually large waves with scaled features and proportions quite similar to the largest wave in WACSIS, often referred to as freak or rogue waves. The presence of second-order bound waves phase locked to the freely propagating linear waves enhances this process.

4. Marginal distributions

The marginal PDs describing ξ and ϕ are given by

$$p_\xi = \int_{-\pi}^{\pi} p_{\phi\xi} d\phi = \xi \exp(-\xi^2/2), \tag{5}$$

$$p_\phi = \int_0^\infty p_{\phi\xi} d\xi = \frac{1}{2\pi} \left(1 - \frac{\lambda_3}{6} \sqrt{\frac{\pi}{2}} \cos\phi \right). \tag{6}$$

Evidently, p_ξ is of the Rayleigh form, as in linear waves. However, the nonlinear surface is vertically skewed with higher sharper crests and shallower more rounded troughs. Accordingly, envelope heights are higher over wave crests and shallower over the troughs. Such second-order distortions do not affect the marginal distri-

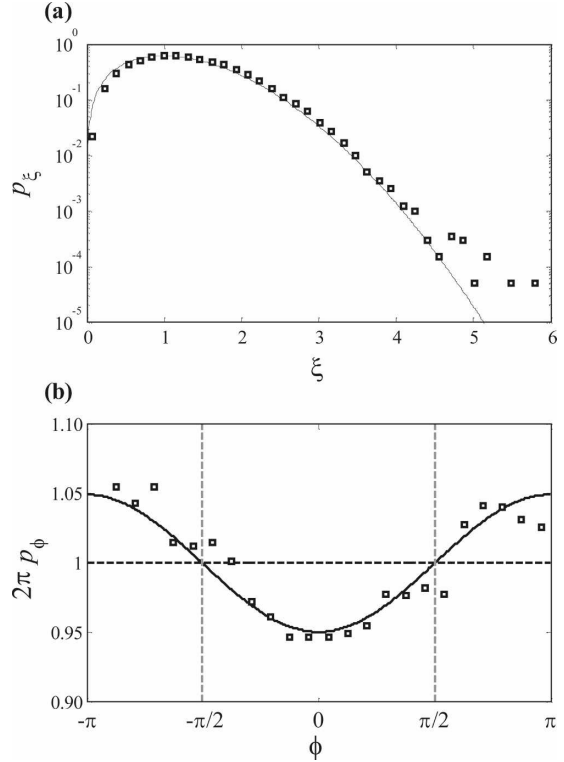


FIG. 6. The marginal densities of (a) wave envelopes and (b) wave phases: WACSIS data compared to Eqs. (5) and (6) (solid lines).

bution of wave envelopes. But, higher-order effects, in particular third-order modulational instabilities induced by four-wave quasi-resonant interactions among free waves, can because they tend to amplify the wave envelope over both wave crests and troughs symmetrically. This tendency is predicted by the nonlinear Schrödinger (NLS) equation or its modified form, the Dysthe equation (Dysthe et al. 2003). As a result, p_ξ can deviate noticeably from the Rayleigh form in a systematic pattern when $\xi > 2$ (Socquet-Juglard et al. 2005; Mori et al. 2007; Fedele 2008). However, Fig. 6 does not suggest such a pattern, and the WACSIS data compares favorably with Eqs. (5) and (6) for the most part. Discrepancies between the envelopes observed and p_ξ do appear for $\xi > 4$ as the data become sparse.

Clearly, $\eta > 0$ for $|\phi| \leq \pi/2$, and $\eta \leq 0$ otherwise. Thus, from Eq. (6),

$$P^+ \equiv \Pr\{\eta > 0\} = \int_{|\phi| \leq \pi/2} p_\phi d\phi = \frac{1}{2} \left(1 - \frac{\lambda_3}{3\sqrt{2\pi}} \right), \tag{7}$$

$$P^- \equiv \Pr\{\eta \leq 0\} = 1 - P^+ = \frac{1}{2} \left(1 + \frac{\lambda_3}{3\sqrt{2\pi}} \right). \tag{8}$$

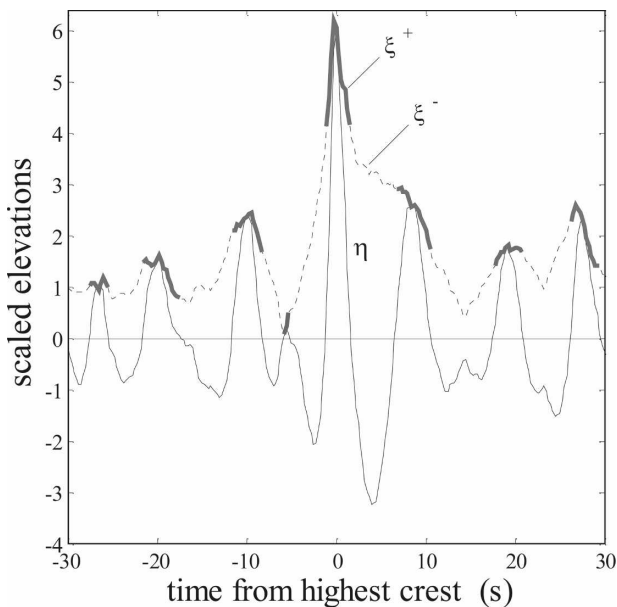


FIG. 7. Sections ξ^+ and ξ^- of the wave envelope ξ coincident with, respectively, the crest ($\eta > 0$) and trough ($\eta \leq 0$) segments of the surface profile η .

The same results also follow from the distribution of η expressed in a Gram–Charlier series to $O(\lambda_3)$ (Longuet-Higgins 1963). Evidently, $P^- > 1/2$ and $P^+ < 1/2$ for $\lambda_3 > 0$, implying that the sea surface stays slightly longer below the mean sea level. In a zero-mean time series of surface displacements sampled at a uniform rate, P^+ is simply the ratio of the number of positive samples to the total number. Thus, given P^+ , an estimate of λ_3 easily follows from Eq. (7) rewritten as $\lambda_3 \cong 3\sqrt{2\pi}(1 - 2P^+)$. For $P^+ \cong 0.485$ in WACSIS, this expression gives $\lambda_3 \cong 0.226$, which compares in this case quite favorably with $\lambda_{3\text{avg}} = 0.231$ representing the overall average of 18 half-hourly cubic moments of η .

5. Conditional distributions of envelope

To describe how the wave envelope is modified by the surface skewness, it is necessary to consider the conditional distributions of ξ coincident with the crest ($\eta > 0$) and trough ($\eta \leq 0$) segments of the surface profile, depicted in Fig. 7 as ξ^+ and ξ^- , respectively. The PDs, say, p_{ξ^+} for ξ^+ and p_{ξ^-} for ξ^- , are of the form (see appendix A for derivations)

$$p_{\xi^\pm}(z) = \frac{1}{2P^\pm} \left[1 \pm \frac{\lambda_3}{3\pi} z(z^2 - 4) \right] p_\xi(z). \quad (9)$$

For $z \gg 1$, the corresponding exceedance distribution (ED) $\Pr\{\xi^\pm > z\} \equiv E^\pm$ is given by

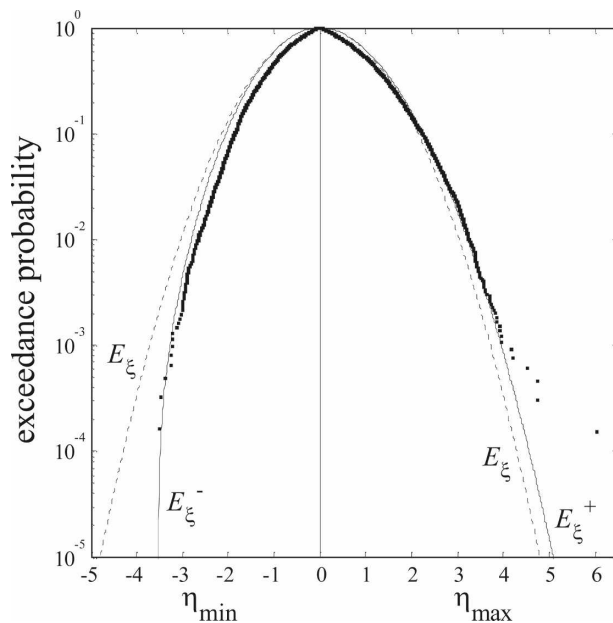


FIG. 8. The distributions of positive maxima and negative minima: WACSIS data (points) compared to the theoretical predictions E_ξ (Rayleigh) and E_{ξ^\pm} of Eq. (10).

$$E_{\xi^\pm}(z) \equiv \frac{E_\xi}{2P^\pm} \left\{ 1 \pm \frac{\lambda_3}{3\pi} [z^3 - z - z^{-1} + O(z^{-3})] \right\}, \quad (10)$$

where $E_\xi \equiv \Pr\{\xi > z\} = \exp(-z^2/2)$ represents the Rayleigh ED appropriate to crest and trough amplitudes in linear narrowband waves. In theory then, E_{ξ^+} and E_{ξ^-} represent similar approximations to the EDs of, respectively, crest and trough amplitudes in nonlinear narrowband waves. Al-Humoud et al. (2002) and Cherneva et al. (2005) explored this possibility and compared E_{ξ^\pm} to measurements representative of relatively broadband waves at deep and shallow waters. These (and likewise similar comparisons with WACSIS, not shown here for economy of space) indicate that although E_{ξ^-} represent trough amplitudes reasonably well, E_{ξ^+} generally tends to underpredict the wave crests.

In general, $\xi^+ \geq \eta_{\text{max}}$ and $-\xi^- \leq \eta_{\text{min}}$, where $\eta_{\text{max}} \equiv \max \eta > 0$ and $\eta_{\text{min}} \equiv \min \eta < 0$ define the local positive maxima and negative minima. Thus, E_{ξ^+} (E_{ξ^-}) represents an upper (lower) bound to the ED of η_{max} (η_{min}) over the low-to-medium range and tends to converge to it over relatively large maxima (minima), just as E_ξ does in linear broadband waves (Cartwright and Longuet-Higgins 1956). As a case in point, Fig. 8 compares the EDs of 6550 positive maxima and 6156 negative minima extracted from WACSIS with the theoret-

ical predictions E_{ξ}^+ and E_{ξ}^- . Both expressions follow from Eq. (10) for $z > 0$, obviously, but E_{ξ}^- is plotted for $z < 0$. It is seen that the WACSIS data follow the theoretically expected trends reasonably well except for the largest five to six positive maxima.

6. Nature of exceedance frequency estimates

The PD of an exceedance estimate, say, E for the j th largest value in a population of n independent identically distributed samples is of the form (cf. Tayfun and Fedele 2007b)

$$p_j = \frac{n!}{(j-1)!(n-j)!} E^{j-1}(1-E)^{n-j}, \quad (11)$$

where $0 \leq E \leq 1$. The mean, standard deviation, and the skewness coefficient of E are given, respectively, by

$$\mu_E = \frac{j}{n+1}, \quad \sigma_E \cong \frac{\sqrt{j}}{n+1}; \quad \frac{\langle (E - \mu_E)^3 \rangle}{\sigma_E^3} \cong \frac{2}{\sqrt{j}}. \quad (12)$$

The expression for μ_E is exact for $j = 1, 2, \dots, n$ and used in plotting the ED estimates in Fig. 8 and similar others to follow later. The standard deviation and skewness coefficient represent approximations valid for large n and $n \gg j$. Thus, the coefficient of variation given by $\delta \equiv \sigma_E/\mu_E \cong 1/\sqrt{j}$ indicates that the variability of the ED estimates for the largest few samples is rather large. In particular, for $j \leq 5$, $\delta > 44\%$, and it increases rapidly to 100% for $j = 1$ irrespective of how large n is. Further, p_j is positively skewed, and the skewness coefficient increases from about 0.82 for $j = 5$ to 2 for $j = 1$. So, the exceedance frequency estimates for the largest few observations tend to be highly variable and skewed toward values greater than μ_E . The latter tendency is of particular relevance for large positive maxima and wave crests since exceptionally large surface displacements in nonlinear seas also tend to occur only above the mean sea level. Consequently, discrepancies often observed between the ED estimates for the largest few surface displacements and theoretical predictions can be explained at least partially in terms of their unstable nature and apparent tendency to occur at relatively higher frequencies than we intuitively expect.

7. Conditional distributions of wave phase

The conditional PD of ϕ , given ξ , follows from Eq. (2) as

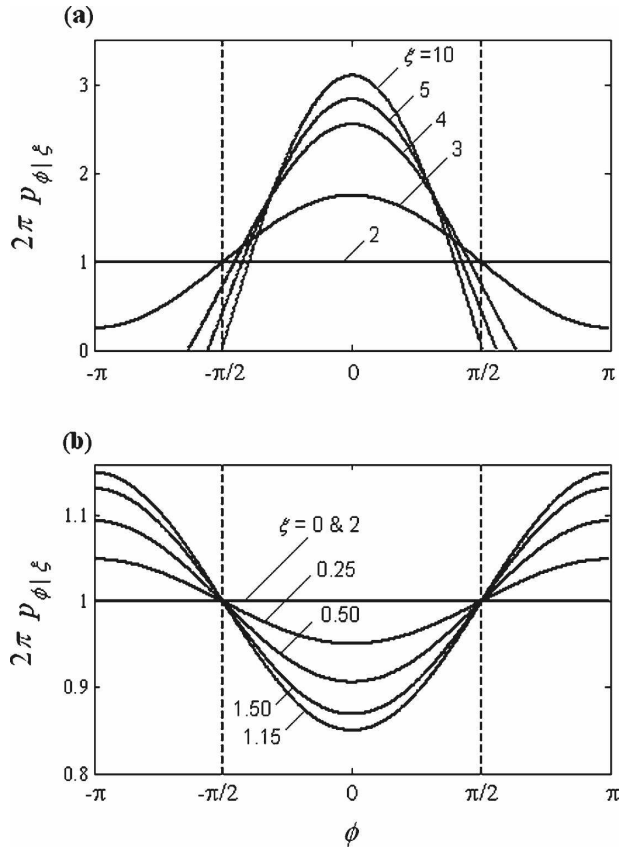


FIG. 9. The variation of conditional density of ϕ , given ξ , with ξ from Eq. (13) for $\lambda_3 = 0.3$: (a) $\xi \geq \xi_s = 2$ and (b) $\xi \leq \xi_s$.

$$p_{\phi|\xi} = \frac{C_1}{2\pi} \left[1 + \frac{\lambda_3}{6} \xi(\xi^2 - 4) \cos\phi \right], \quad |\phi| \leq \phi_c, \quad (13)$$

where

$$C_1 = \begin{cases} 1, & \xi \leq \xi_m, \\ \pi/(\phi_c - \tan\phi_c), & \xi > \xi_m, \end{cases} \quad (14)$$

with $\xi_m > 2$ as in Eq. (4), and

$$\phi_c = \begin{cases} \pi, & 0 < \xi \leq \xi_m, \\ \cos^{-1}[-6/\lambda_3 \xi(\xi^2 - 4)], & \xi > \xi_m. \end{cases} \quad (15)$$

Now, using $\tan\phi_c = \sin\phi_c/\cos\phi_c$ in Eq. (14) and expressing $\sin\phi_c$ in terms of ξ from Eq. (15), it is easily verified that as $\xi \rightarrow \infty$, $\phi_c \rightarrow \pi/2$, and Eq. (13) converges to the limit form

$$p_{\phi|\xi} = (1/2) \cos\phi, \quad |\phi| \leq \pi/2. \quad (16)$$

The variation of $p_{\phi|\xi}$ with ξ is shown in Fig. 9 for $\lambda_3 = 0.3$. It is noticed that $\xi_s = 2$ corresponds to the mean of the 1/3 largest ξ values, traditionally referred to as the significant value. Clearly, $p_{\phi|\xi}$ appears strikingly differ-

ent depending on if $\xi \leq \xi_s$. For $\xi = 0$ and ξ_s , $p_{\phi|\xi} = 1/2\pi$ as in linear waves. For $0 < \xi < 2/\sqrt{3} \cong 1.15$, $p_{\phi|\xi}$ deviates from $1/2\pi$ progressively up to 1.15. As ξ increases further from 1.15 to ξ_s , it converges back to $1/2\pi$. So, for $\xi < \xi_s$, $p_{\phi|\xi}$ has a slight excess of phases over wave troughs, where $\eta < 0$ and a corresponding deficiency elsewhere. However, when $\xi > \xi_s$, the opposite occurs and $p_{\phi|\xi}$ shows an excess of phases over wave crests. In particular, as ξ becomes larger, this excess increases progressively, and $p_{\phi|\xi}$ converges to the limit form in Eq. (16). Physically, the surface stays slightly longer below the mean sea level if $\xi < \xi_s$, whereas if $\xi > \xi_s$, the opposite occurs in an increasingly pronounced manner as ξ becomes larger. The limit form suggests that exceptionally large surface displacements can occur only above the mean sea level. This result is consistent with the WACSIS data of Fig. 5.

In practice, $p_{\phi|\xi}$ can be estimated from a surface time series only if the condition “given ξ ” is approximated as “given $\xi - \Delta\xi < \xi \leq \xi + \Delta\xi$,” where $\Delta\xi$ represents a small increment. The favorable comparisons of Eq. (13) with WACSIS, shown in Fig. 10, are based on this approximation, using $\Delta\xi = 0.2$ for $\xi = 2, 3$ and 3.5.

The PD of ϕ , conditional on $A \equiv \{\xi > \xi_0\}$, is given by

$$p_{\phi|A} = \int_{\xi_0}^{\infty} p_{\phi\xi} d\xi \bigg/ \int_{\xi_0}^{\infty} p_{\xi} d\xi = \frac{C_2}{2\pi} \left[1 + \frac{\lambda_3}{6} f(\xi_0) \cos\phi \right], \tag{17}$$

where $|\phi| \leq \phi^*$ and

$$f(\xi_0) \equiv \xi_0^3 - \xi_0 - \sqrt{\frac{\pi}{2}} \exp\left(\frac{\xi_0^2}{2}\right) \operatorname{erfc}\left(\frac{\xi_0}{\sqrt{2}}\right), \tag{18}$$

$$C_2 = \begin{cases} 1, & \xi_0 \leq \xi_0^* \\ \pi/(\phi^* - \tan\phi^*), & \xi_0 > \xi_0^* \end{cases} \tag{19}$$

with $\xi_0^* > 1.218$ in general such that $f(\xi_0^*) = 6/\lambda_3$, and

$$\phi^* = \begin{cases} \pi, & 0 < \xi_0 \leq \xi_0^* \\ \cos^{-1}[-6/\lambda_3 f(\xi_0)], & \xi_0 > \xi_0^* \end{cases} \tag{20}$$

In this case, ξ_0^* follows as an iterative solution from

$$x_{j+1} = \left[\frac{6}{\lambda_3} + x_j + \sqrt{\frac{\pi}{2}} \exp\left(\frac{x_j^2}{2}\right) \operatorname{erfc}\left(\frac{x_j}{\sqrt{2}}\right) \right]^{1/3} \tag{21}$$

for $j = 0, 1, 2, \dots$, and $x_0 \geq 0$.

Finally, the PD of ϕ , conditional on $B \equiv \{\xi \leq \xi_0\}$, is given by

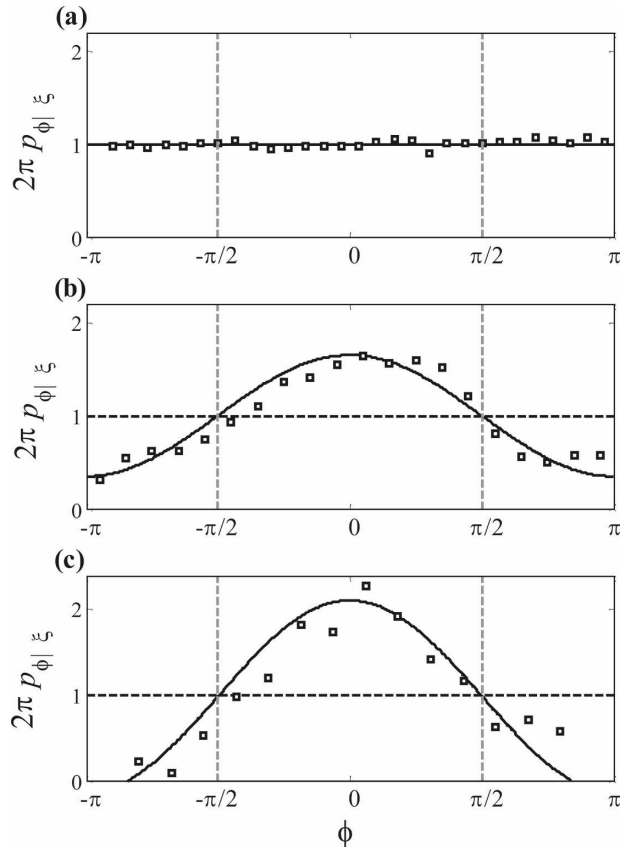


FIG. 10. The conditional density of ϕ , given ξ : WACSIS data compared to predictions (solid lines) from Eq. (13) for (a) $\xi = 2$, (b) $\xi = 3$, and (c) $\xi = 3.5$.

$$p_{\phi|B} = \int_0^{\xi_0} p_{\phi\xi} d\xi \bigg/ \int_0^{\xi_0} p_{\xi} d\xi = \frac{1}{2\pi} \left[1 - \frac{\lambda_3}{6} w(\xi_0) \cos\phi \right], \tag{22}$$

where $\xi_0 > 0$, $|\phi| \leq \pi$, and

$$w(\xi_0) = \frac{\xi_0^3 - \xi_0 + \sqrt{\pi/2} \exp(\xi_0^2/2) \operatorname{erf}(\xi_0/\sqrt{2})}{\exp(\xi_0^2/2) - 1}. \tag{23}$$

The variations of f and w with ξ_0 are shown in Fig. 11. It is seen that $w \geq 0$ with a maximum 2.511 at $\xi_0 \cong 1.539$, whereas $f \leq 0$ for $0 \leq \xi_0 < 1.218$ and $f > 0$, otherwise. As $\xi_0 \rightarrow 0$, $f \rightarrow -\sqrt{\pi/2}$, and $p_{\phi|A} \rightarrow p_{\phi}$ of Eq. (6). As $\xi_0 \rightarrow \infty$, $p_{\phi|A} \rightarrow (1/2) \cos\phi$ of Eq. (16); and, if $\xi_0 \cong 1.218$, then $p_{\phi|A} \rightarrow 1/2\pi$ for any λ_3 . For $\xi_0 \ll 1$, $w \approx 0$, and $p_{\phi|B} \approx 1/2\pi$. If, however, $\xi_0 > 4$ approximately, then $w \rightarrow \sqrt{\pi/2}$ and so $p_{\phi|B} \rightarrow p_{\phi}$ of Eq. (6) also.

Figure 12 illustrates the variation of $p_{\phi|A}$ with ξ_0 for $\lambda_3 = 0.3$, and in Fig. 13 its comparisons with WACSIS. Similarly, Figs. 14 and 15 show the variation of $p_{\phi|B}$ and

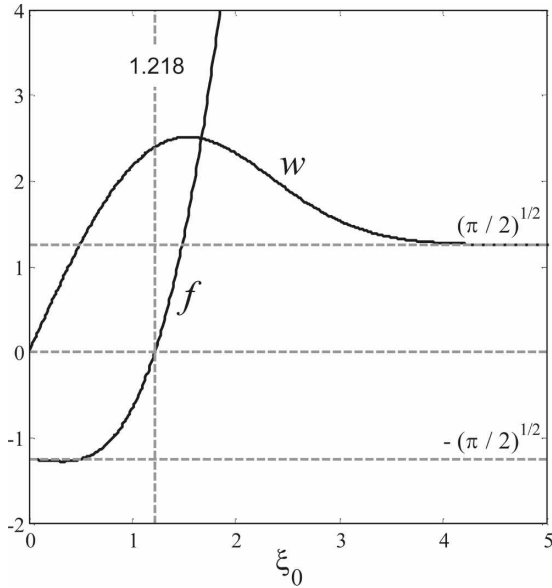


FIG. 11. The variations of functions f and w with ξ_0 from Eqs. (18) and (23), respectively.

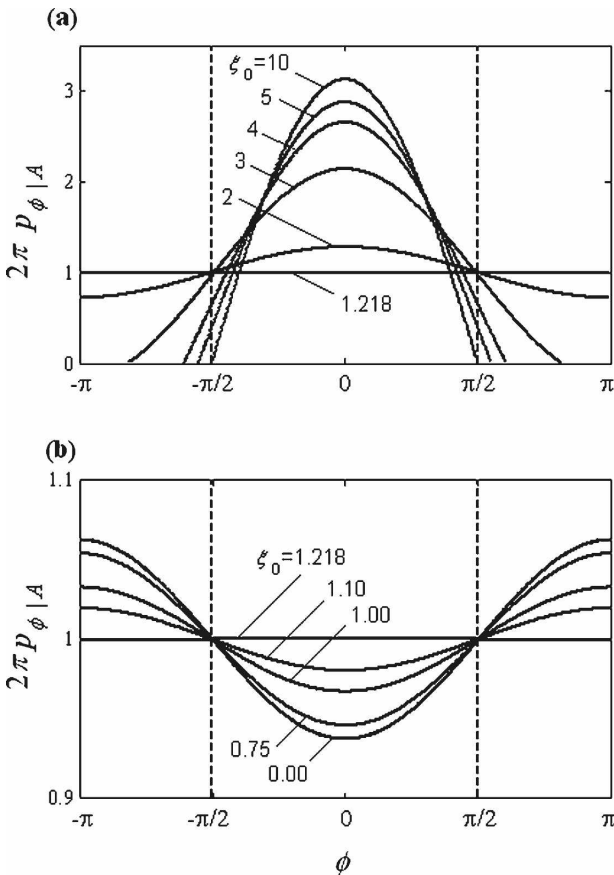


FIG. 12. The variation of conditional density of ϕ , given $A \equiv \{\xi > \xi_0\}$, with ξ_0 from Eq. (17) (solid lines) for $\lambda_3 = 0.3$: (a) $\xi_0 \geq 1.218$ and (b) $\xi_0 \leq 1.218$.

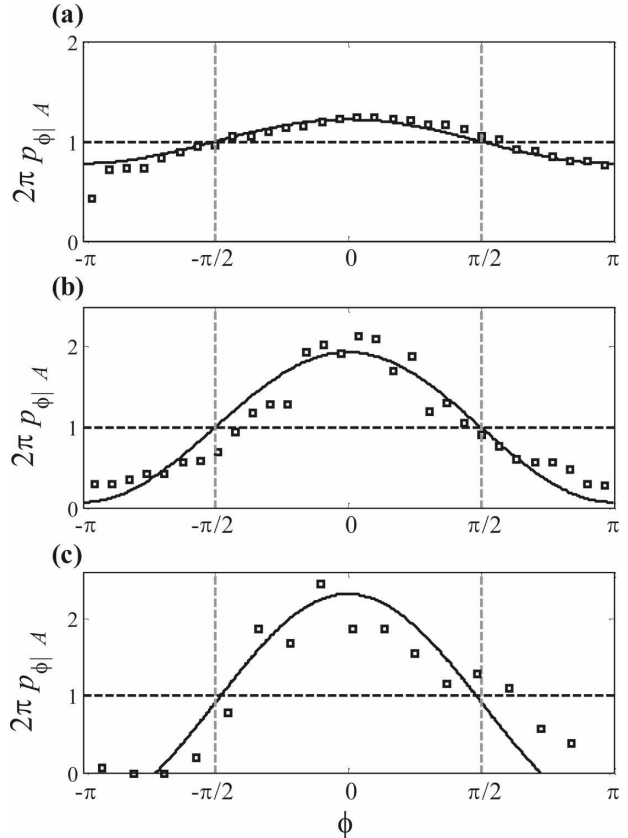


FIG. 13. The conditional density of ϕ , given $A \equiv \{\xi > \xi_0\}$: WACSIS data compared to Eq. (17) (solid lines) for (a) $\xi_0 = \xi_c = 2$, (b) $\xi_0 = 3$, and (c) $\xi_0 = 3.5$.

its comparisons with WACSIS, respectively. Both sets of comparisons confirm the relative validity of the theoretical expressions.

8. Large surface displacements

To elaborate the expectation that very large displacements occur only above the mean sea level by way of probabilistic formalism, let $P_A^+ \equiv \Pr\{\eta > 0|A\}$ with $A \equiv \{\xi > \xi_0\}$ as before. Since $\eta > 0$ occurs for $|\phi| \leq \pi/2$, the preceding conditional probability follows easily from Eq. (17) by integrating it with respect to ϕ over $(-\pi/2, \pi/2)$ as

$$\begin{aligned}
 P_A^+ &= \frac{C_2}{2} \left\{ 1 + \frac{\lambda_3}{3\pi} \left[\xi_0^3 - \xi_0 \right. \right. \\
 &\quad \left. \left. - \sqrt{\frac{\pi}{2}} \exp\left(\frac{\xi_0^2}{2}\right) \operatorname{erfc}\left(\frac{\xi_0}{\sqrt{2}}\right) \right] \right\} \\
 &= \frac{C_2}{2} \left\{ 1 + \frac{\lambda_3}{3\pi} [\xi_0^3 - \xi_0 - \xi_0^{-1} + O(\xi_0^{-3})] \right\};
 \end{aligned}$$

$$\xi_0 \gg 1.$$

(24)

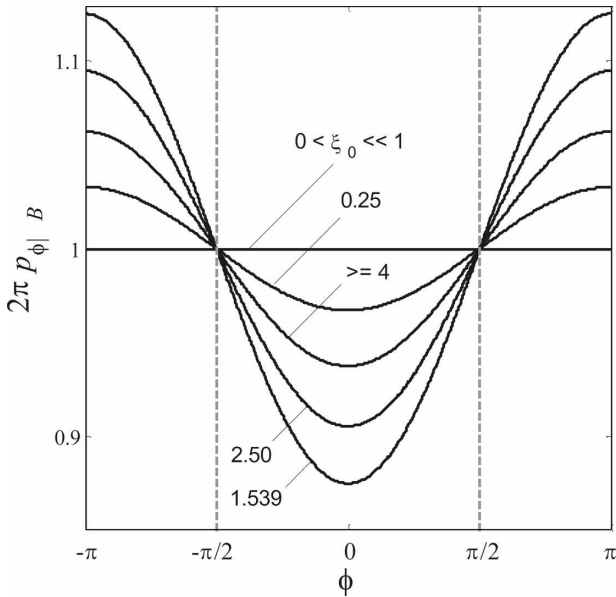


FIG. 14. The variation of conditional density of ϕ , given $B \equiv \{\xi \leq \xi_0\}$, with ξ_0 from Eq. (22) (solid lines) for $\lambda_3 = 0.3$.

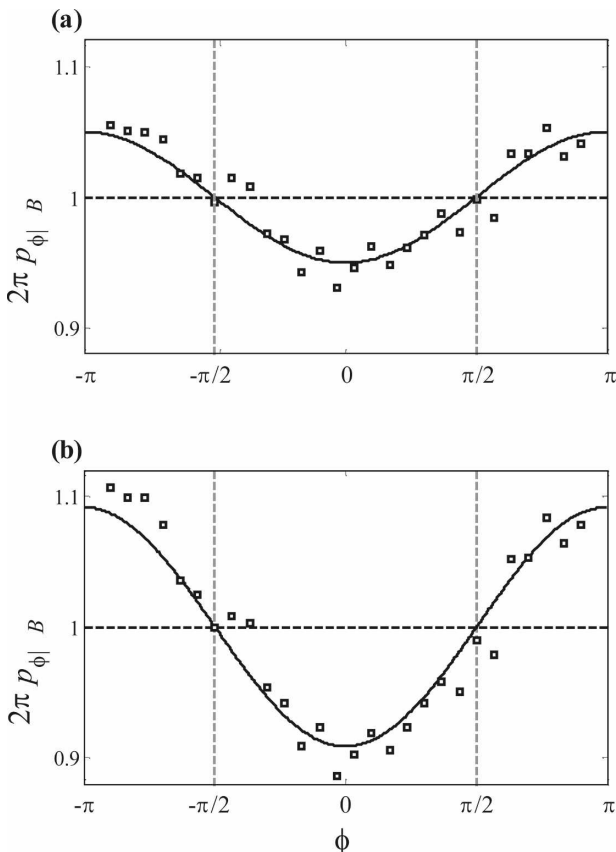


FIG. 15. The conditional density of ϕ , given $B \equiv \{\xi \leq \xi_0\}$: WACSIS data compared to Eq. (22) (solid lines) for (a) $\xi_0 = 5$ and (b) $\xi_0 = 2$.

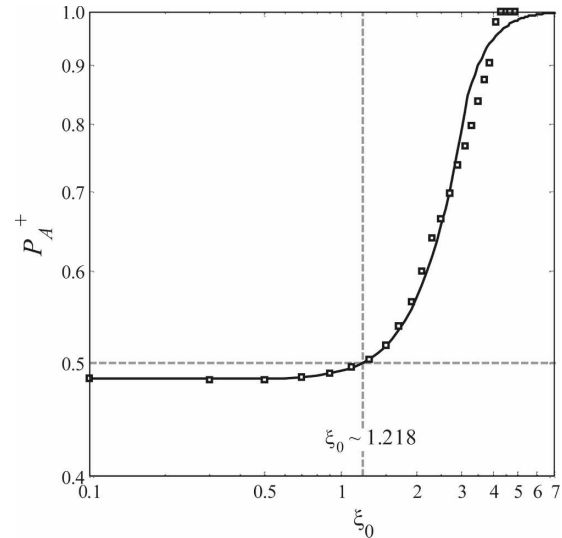


FIG. 16. Conditional probability $P_A^+ = \Pr\{\eta > 0 | \xi > \xi_0\}$: WACSIS data compared to Eq. (22) (solid line).

This expression compares with WACSIS quite favorably, as shown in Fig. 16. Obviously, $P_A^+ \equiv \Pr\{\eta > 0 | A\}$ is the complement of $P_A^- \equiv \Pr\{\eta \leq 0 | A\}$, not shown in this figure. It is also noticed that for $\xi_0 > 4$, approximately, $P_A^+ \approx 1$, and thus $P_A^- \approx 0$ in WACSIS. This is likewise predicted reasonably well by the limit behavior of Eq. (24) for large ξ_0 .

9. Large waves

a. Nature of large waves and associated phases

Let m_j ($j = 0, 1, 2, \dots$) denote the ordinary spectral moments. Thus, $m_0 = \sigma^2$, $\omega_m = m_1/m_0 \equiv$ spectral mean frequency, and $v = [(m_0/m_2/m_1^2) - 1]^{1/2} \equiv$ spectral bandwidth. To the leading order of approximation, the conditional distribution of $\dot{\phi} \equiv \partial\phi/\partial t$, given ξ , is Gaussian with mean ω_m and standard deviation $v\omega_m/\xi$ (Longuet-Higgins 1957). Second-order nonlinearities introduce corrections of $O(\lambda_3)$ in these statistics, but the actual comparisons with WACSIS indicate that these are relatively insignificant and therefore ignored in the present discussion. It follows, then, that for $\xi \gg v$,

$$\Pr\{\dot{\phi} \leq 0\} = (1/2)\text{erfc}(\xi/v\sqrt{2}),$$

$$\approx (v/\xi\sqrt{2\pi}) \exp(-\xi^2/2v^2) \approx 0.$$

Thus, if ξ is sufficiently large, it is nearly certain that $\dot{\phi} > 0$ and ϕ increase monotonously. This tends to occur in WACSIS in time intervals during which $\xi > \xi_s \approx 4v$ approximately. Physically, the corresponding surface displacements and thus relatively large waves appear more regular or narrow band in the sense that they do

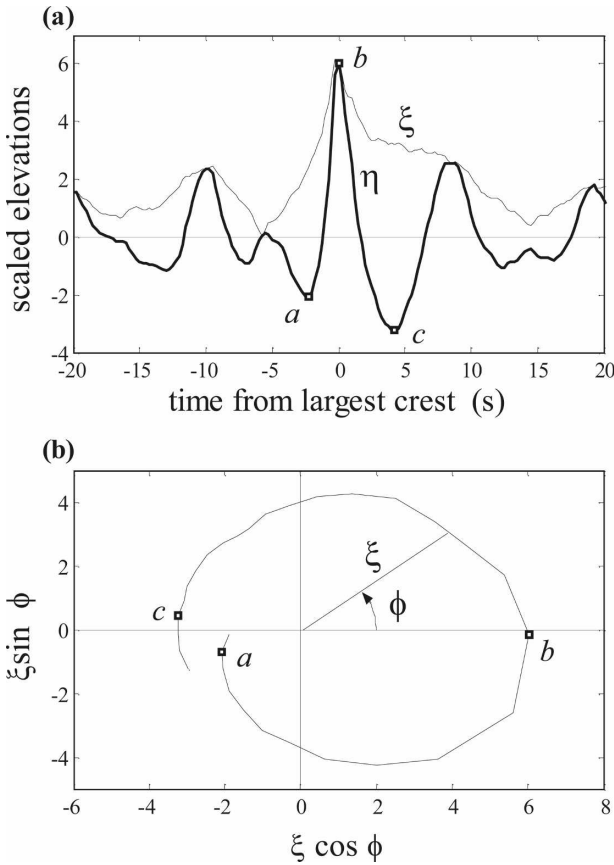


FIG. 17. (a) The surface profile η and (b) the variation of wave phase ϕ around the largest wave (abc) of WACSIS, where $\xi > \xi_s = 2$, approximately.

not display any secondary maxima or minima but a single crest preceded by a relatively deep trough, as in Fig. 17, where $\xi > \xi_s$ around the largest wave of WACSIS. Secondary extremes can occur only in time intervals during which $\phi < 0$ and phase reversals occur, as shown in Fig. 18, for a short segment of the surface time series near the beginning of WACSIS, where $\xi < \xi_s$, approximately.

b. Statistics of wave heights, crests, and troughs

In linear waves, the expected surface profile around a large wave crest is described by the conditional mean (cf. Lindgren 1972; Phillips et al. 1993; Boccotti 2000)

$$\langle \eta(t) | \eta_0 \gg 1 \rangle = \xi \rho(t), \tag{25}$$

where ρ is the normalized covariance kernel of η . As $t \rightarrow 0$, $\rho \rightarrow 1$, and $\eta_0 \equiv \eta(0) \rightarrow \xi$, which is the large wave crest. Further, if t^* denotes the time at which the first minimum $\rho(t^*) \equiv a < 0$ of ρ occurs, then (Boccotti 2000)

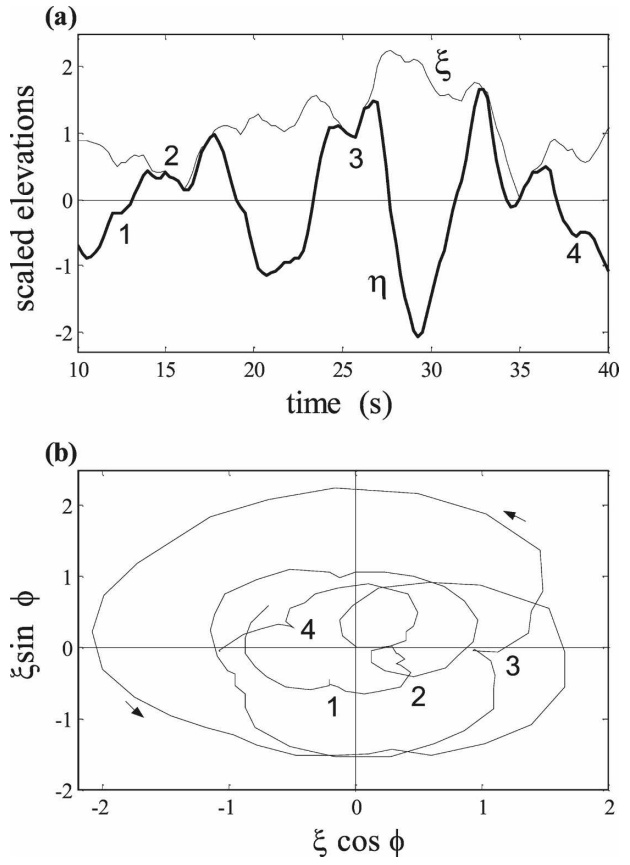


FIG. 18. A short segment of the WACSIS surface profile series where $\xi < \xi_s = 2$, approximately: (a) occurrences of secondary maxima and minima and (b) associated wave-phase reversals (shown as 1, 2, 3, and 4, where $\phi < 0$ locally).

$$\eta_0 \equiv \xi \cong h/(1 - a), \tag{26}$$

with h defined as the zero up or down crossing wave height scaled with σ . Second-order corrections modify Eq. (25) as (Tayfun and Fedele 2007a; see also appendix B)

$$\langle \eta(t) | \eta_0 \gg 1 \rangle = \xi \rho(t) + \frac{\lambda(t)}{6} \xi^2, \tag{27}$$

where

$$\eta_0 \equiv \xi_c = \xi + \frac{\lambda_3}{6} \xi^2, \tag{28}$$

represents the second-order wave crest, and $\lambda(t)$ is a dimensionless kernel described in appendix B. In general though, $\lambda(0) = \lambda_3$ and $\rho(0) = 1$. As a result, Eq. (27) converges to Eq. (28) as $t \rightarrow 0$.

The theoretical expressions describing the EDs of h , ξ_c , and the corresponding second-order trough amplitude, say, ξ_t , are critically reviewed in Tayfun and

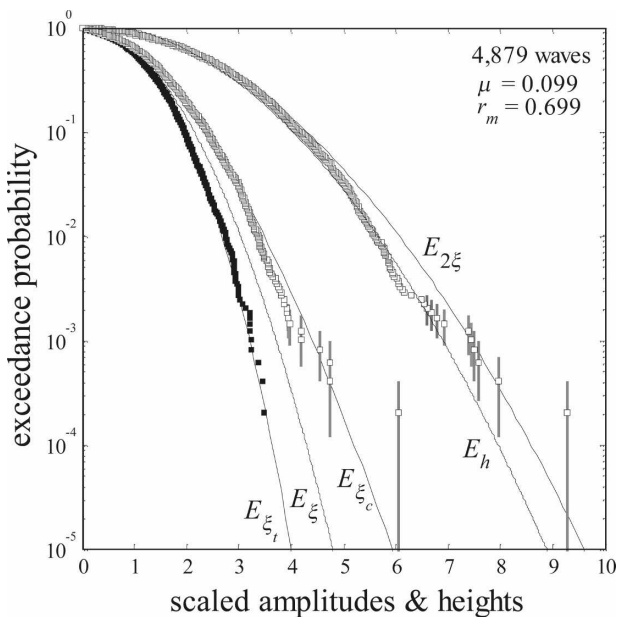


FIG. 19. Exceedance distributions of zero up-crossing wave heights (h), crest (ξ_c) and trough (ξ_t) amplitudes: WACSIS data compared to E_h , E_{ξ_c} , and E_{ξ_t} [Eqs. (29), (30), and (31)], E_{ξ} (Rayleigh ED) for linear crest and trough amplitudes, and $E_{2\xi}$ (Rayleigh ED) for narrowband wave heights ($h \cong 2\xi$). Vertical lines indicate the theoretical $\pm\sigma_E$ bands [Eq. (12)].

Fedele (2007b). These include the following expressions, valid for large waves:

$$E_h = \sqrt{\frac{1+r_m}{2r_m}} \exp\left[-\frac{h^2}{4(1+r_m)}\right], \quad (29)$$

$$E_{\xi_c} = \exp\left[-\frac{1}{2}\left(\frac{\sqrt{1+2\mu\xi_c}-1}{\mu}\right)^2\right], \quad (30)$$

$$E_{\xi_t} = \exp\left[-\frac{1}{2}\left(\xi_t + \frac{1}{2}\mu\xi_t^2\right)^2\right], \quad (31)$$

where r_m and μ represent dimensionless wave height and steepness parameters, respectively (cf. Tayfun 2006; Tayfun and Fedele 2007b). For WACSIS, $r_m = 0.699$ and $\mu = 0.099$ ($\mu \equiv \mu_{F2}$ in Tayfun 2006). Figure 19 compares the WACSIS data with E_h , E_{ξ_c} , E_{ξ_t} , and also with the narrowband Rayleigh limits, namely $E_{\xi} = \exp(-\xi^2/2)$ for linear crest and trough amplitudes and $E_{2\xi} = \exp(-h^2/8)$ for wave heights, on the assumption $h \cong 2\xi$. The variability of the ED estimates for the largest few values are indicated by $\pm\sigma_E$ bands in the same figure. Evidently, neither E_{ξ} nor $E_{2\xi}$ represents the observed trends quite satisfactorily. Nevertheless, it appears that the heights of larger waves tend to $E_{2\xi}$, plausibly because large waves are more like narrowband waves and, to some extent, due to second-order correc-

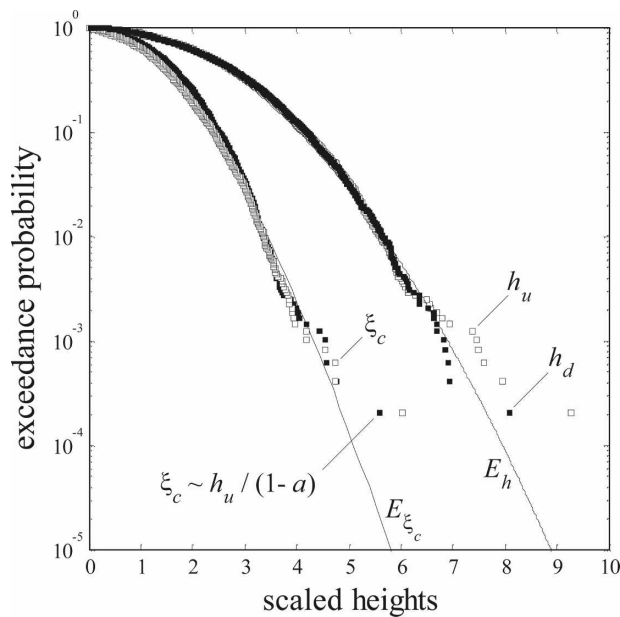


FIG. 20. Exceedance distributions of zero up- and down-crossing wave heights (h_u and h_d), crests (ξ_c), and crests estimated from $h_u/(1-a)$ [Eq. (26)] compared to E_h and E_{ξ_c} [Eqs. (29) and (30)].

tions (Tayfun and Fedele 2007b). In contrast, E_{ξ_t} describes the trough amplitudes of all waves fairly accurately. The comparisons between E_h and the observed wave heights and, similarly, between E_{ξ_c} and the wave crests are also favorable for the most part, but some discrepancies appear over large waves. This is particularly so for the largest wave whose height and crest exceed all the theoretical distributions noticeably. As elaborated previously, such discrepancies do appear every so often at least partially because of the relatively unstable and positively skewed nature of the exceedance frequency estimates associated with large surface displacements.

In nonlinear waves, wave heights derived from zero downcrossings can differ noticeably from the zero up-crossing wave heights over large waves. Wave crests remain the same in either definition, but the zero down-crossing wave height is the sum of a crest and the preceding trough amplitude, which tends to be typically shallower than the trough amplitude following the same crest. Thus, zero downcrossing wave heights are often smaller than the corresponding zero upcrossing heights over large waves. This trend is seen clearly in the WACSIS comparisons of Fig. 20, where the largest zero downcrossing wave height observed is 8.10 as compared to 9.27 for the largest zero upcrossing wave height. The same figure also shows the crest heights derived from the zero upcrossing wave heights via Eq. (26). Appar-

ently, these compare reasonably well with the nonlinear crest heights actually observed in WACSIS. In theory, Eq. (26) is valid for linear waves, but using the second-order equation (28) instead yields in this case somewhat larger crest heights than the actual (not shown in the figure). Nonetheless, both expressions have some relevance in exploring possible upper limits to wave crests.

c. Miche–Stokes limits

How large surface displacements and thus wave heights and crests can really become is a difficult question to answer, particularly based on the present second-order model and higher-order approximations because they ignore surface stresses, wave breaking, and turbulent dissipation. Yet, wind wave spectra tend to a ω^{-4} power law over high frequencies, implying that the surface gradients are discontinuous in the mean-square sense. Physically, this means that some waves reach a limiting steepness, display sharply cornered crests, and some break, forming whitecaps. An approximate upper limit to wave steepness and thus to wave heights is defined by the Miche limit (Miche 1944), expressed in the present notation by

$$h_{\max} = \frac{2\pi \tanh kd}{7} \frac{1}{\sigma k}, \tag{32}$$

where $k \equiv$ wavenumber and $d \equiv$ mean water depth. As $d \rightarrow \infty$, h_{\max} converges to the well-known Stokes limit.

The applicability of the Miche–Stokes-type limits to irregular waves has been the subject of numerous studies, reviewed in Tulin and Li (1992, and references therein). The Miche–Stokes limits or their various refinements do not appear as consistent indicators of wave breaking or its inception for irregular waves. However, they do indicate an upper bound to the heights of large waves, breaking or otherwise. Again, this may be so at least partially because large waves behave more like regular waves. Larger wave heights in WACSIS, shown at the top of Fig. 21, versus the corresponding scaled zero upcrossing periods $\tau \equiv T/T_m$, where $T_m \equiv 2\pi/\omega_m$, do not violate Eq. (32). Similarly, the bottom of the same figure shows the scatter of wave crests and periods in comparison with the approximate limits, $\xi_{c,\max 1}$ and $\xi_{c,\max 2}$, which follow from Eqs. (26) and (28), respectively, by replacing h with h_{\max} of Eq. (32) as

$$\xi_{c,\max 1} \cong h_{\max}/(1 - a) \tag{33}$$

and

$$\xi_{c,\max 2} \cong \frac{h_{\max}}{1 - a} \left(1 + \frac{\lambda_3}{6} \frac{h_{\max}}{1 - a} \right). \tag{34}$$

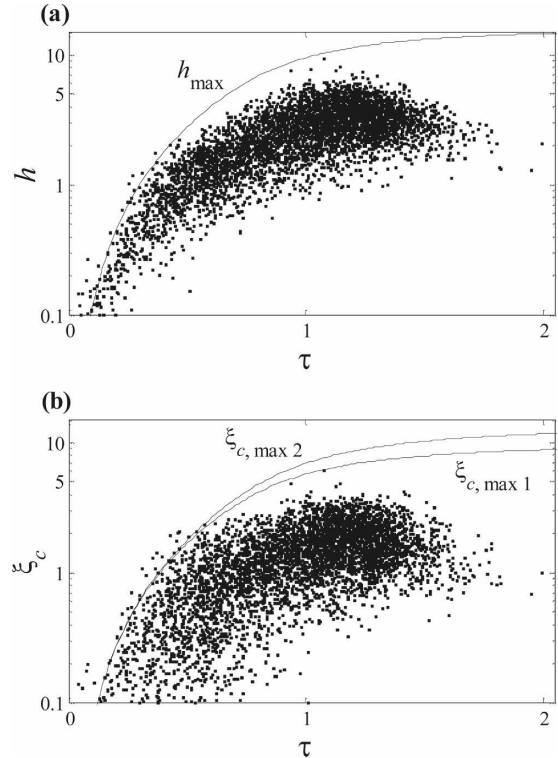


FIG. 21. WACSIS: Scatter diagrams of (a) zero up-crossing wave heights h and (b) wave crests ξ_c vs zero up-crossing wave periods $\tau \equiv T/T_m$ ($T_m = 6.965$ s) compared to the upper limits in Eqs. (32), (33), and (34) (solid lines).

With $a = -0.661$ as an overall average in WACSIS, neither one of these, not even the less conservative approximation in Eq. (33), is violated by any large wave crest. If $\xi < \xi_s$, approximately, some waves do exceed all the upper limits somewhat. So, the Miche–Stokes limits appear to be valid for relatively large waves as they behave more like regular waves.

10. Third-order nonlinear corrections

a. Modulational instabilities

In weakly nonlinear waves, third-order corrections to surface displacements, wave envelopes, and phases are all $O(\lambda_3^2)$ typically and, thus, negligible relative to second-order corrections (Longuet-Higgins 1963; Tayfun 1990, 1994). This has been assumed so in developing the present theoretical approximations. The favorable nature of the WACSIS comparisons validates this assumption to a great extent. However, third-order modulational instabilities can under certain conditions become at least as significant as second-order effects, causing surface features and associated statistics to deviate from the second-order predictions. Such instabili-

ties are generated in wave tanks or numerically simulated via NLS under somewhat contrived conditions generally requiring that waves be long crested and rather narrowband (Socquet-Juglard et al. 2005; Onorato et al. 2006; Mori and Janssen 2006; Gramstad and Trulsen 2007; Mori et al. 2007). It is questionable if these conditions represent directionally spread broadband oceanic wind waves. What appears certain, however, is that NLS-type instabilities are not expected to occur if the relative water depth $k_p d$, where $k_p \equiv$ wave-number at the spectrum peak, is less than 1.363 (cf. Onorato et al. 2006). This has particular relevance for WACSIS as it represents waves in relatively shallow water. Indeed, an analysis of k_p values derived from the spectra of half-hourly running series in WACSIS leads to $k_p d$ values, all of which lie below the threshold 1.363, as shown in Fig. 22. Thus, it is unlikely if NLS-type modulational instabilities have any relevance in WACSIS.

b. Third-order effects on the statistics of wave heights, envelopes, and phases

As briefly mentioned in section 4, third-order distortions observed in the statistics of nonlinear waves, numerically simulated or mechanically generated in wave tanks, follow a fairly predictable and systematic pattern that displays a progressive excess of large waves, starting at wave height, envelope, and crest levels near their significant values. This is predicted reasonably well by third-order Gram–Charlier series describing the statistics of long-crested narrowband waves (Tayfun 1990; Mori et al. 2007; Tayfun and Fedele 2007b). In particular, the marginal ED of the wave envelope ξ is given by

$$E_\xi = \exp(-\xi^2/2) \left[1 + \frac{\Lambda}{64} \xi^2(\xi^2 - 4) \right], \quad (35)$$

where $\Lambda \equiv \lambda_{40} + 2\lambda_{22} + \lambda_{04}$ and, for $n = 0, 1, \dots, 4$,

$$\lambda_{(4-n)n} \equiv \langle \hat{\eta}^{4-n} \hat{\eta}^n \rangle + (-1)^{n/2} (3-n)(n-1), \quad (36)$$

$$n = 0, 1, \dots, 4$$

represent the fourth-order normalized joint cumulants. As $v \rightarrow 0$, the marginal ED of the wave heights defined as $h \equiv 2\xi$ easily follows by a change of variables from (35) as

$$E_h = \exp(-h^2/8) \left[1 + \frac{\Lambda}{1024} h^2(h^2 - 16) \right]. \quad (37)$$

The leading terms in Eqs. (35) and (37) represent different forms of the Rayleigh ED, valid in general for

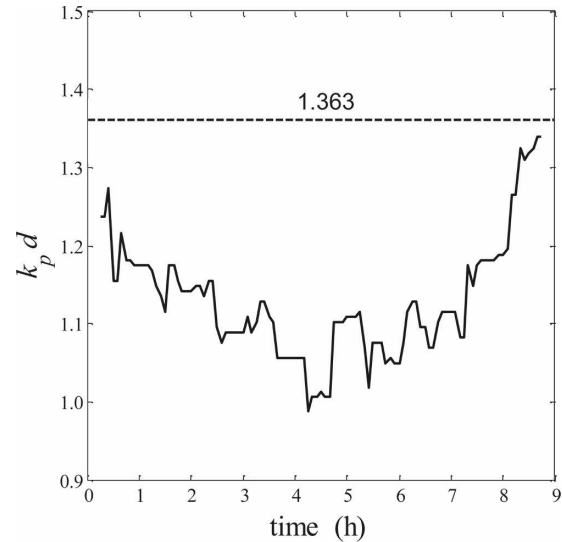


FIG. 22. WACSIS: the temporal variation of relative water depth $k_p d$ derived from the spectral estimates of half-hourly running surface series (avg $k_p d = 1.13$).

Eq. (35) but only for rather narrowband waves in the latter case. The significant envelope and wave heights are $\xi_s = 2$ and $h_s = 4$. So, $\Pr\{\xi > \xi_s\} = \Pr\{h > h_s\} \cong 13.5\%$ in either case. Further, notice that if $\Lambda = O(1)$, $\xi > \xi_s$, and $h > h_s$, then $E_\xi/\exp(-\xi^2/2) > 1$ and $E_h/\exp(-h^2/8) > 1$, and both ratios increase monotonously. Thus, Eqs. (35) and (37) and similar approximations in Tayfun and Fedele (2007b) for wave crests and troughs all suggest that over the range where significant values are exceeded by at least 13.5% largest waves, third-order instabilities systematically amplify wave envelopes, heights, and crest and trough amplitudes noticeably and, if $\Lambda > 1$, approximately, well beyond the levels predicted by the linear or second-order approximations. None of the present comparisons displays any data trend even remotely similar to this systematic pattern, which requires a much larger population of unusually large waves than just a few. For WACSIS as a whole, $\lambda_{40} \cong 0.039$, $\lambda_{22} \cong 0.000$, and $\Lambda \cong -0.008$. Not surprisingly, these are all of $O(\lambda_3^2)$ and negligible in conformity with the weakly nonlinear second-order theory.

For wave phases, third-order corrections similarly contribute to Eq. (6) several additional terms proportional to λ_{mn} , where $m, n = 0, 1, \dots, 4$, such that $m + n = 4$. As a result, the marginal PD of ϕ assumes a somewhat unwieldy form in the most general case. However, if $\lambda_{31} = \lambda_{13} = 0$ as it appears to be the case in relatively long-crested narrowband waves (cf. Tayfun 1990; Mori and Janssen 2006), then Eq. (6) is modified as (Tayfun 1990)

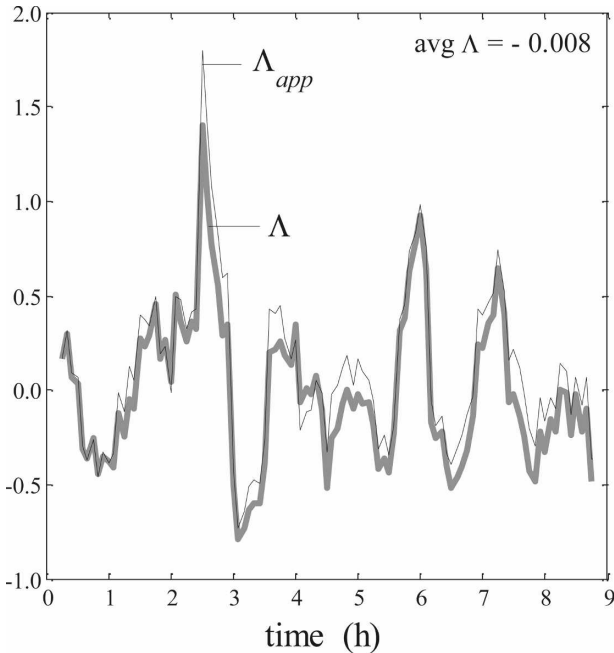


FIG. 23. WACSIS: temporal variations of $\Lambda \equiv \lambda_{40} + 2\lambda_{22} + \lambda_{04}$ and $\Lambda_{app} \equiv 8\lambda_{40}/3$ estimated from half-hourly running averages.

$$\begin{aligned}
 2\pi p_\phi = & 1 - \frac{\lambda_3}{6} \sqrt{\frac{\pi}{2}} \cos\phi \\
 & + \frac{\lambda_{40}}{24} (8 \cos^4\phi - 12 \cos^2\phi + 3) \\
 & + \frac{\lambda_{22}}{4} (8 \cos^2\phi \sin^2\phi - 1) \\
 & + \frac{\lambda_{04}}{24} (8 \sin^4\phi - 12 \sin^2\phi + 3). \quad (38)
 \end{aligned}$$

If $\lambda_{22} \cong \lambda_{40}/3$ and $\lambda_{04} \cong \lambda_{40}$ also, as in Mori & Janssen (2006), then $\Lambda \rightarrow \Lambda_{app} \equiv 8\lambda_{40}/3$ and Eq. (38) converges to Eq. (6) appropriate to second-order waves. For WACSIS as a whole, $\lambda_{31} \cong \lambda_{31} \cong -0.006$ and $\Lambda \cong \Lambda_{app}$, very nearly, as shown in Fig. 23. So, Eq. (38) does in fact reduce to Eq. (6) as a further confirmation that third-order effects do not affect the wave phase statistics of WACSIS.

c. An alternate approach

The premise that surface displacements are rendered vertically skew mainly by second-order bound modes offers an alternate approach for exploring if any third-order NLS-type instabilities are manifest in a wind wave record. Generally, second-order bound modes do not significantly affect the fourth-order cumulants, whereas third-order modulational instabilities can since

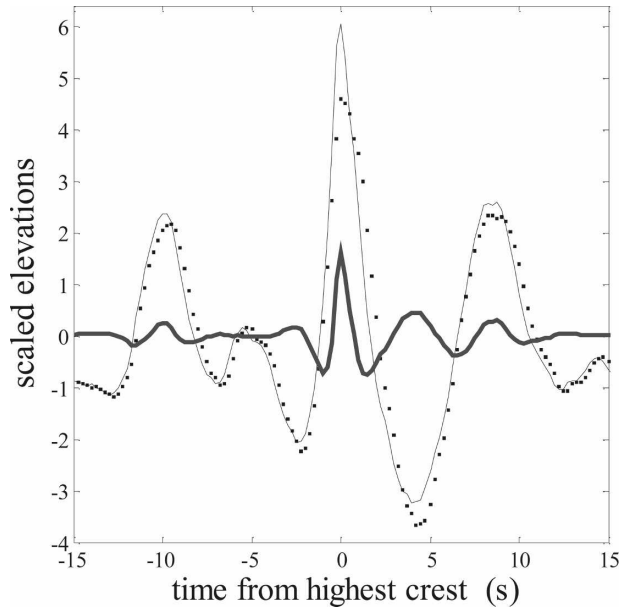


FIG. 24. The surface profile η (thin solid line), nonskew series $\tilde{\eta}$ (points), and second-order correction $\lambda_3(\eta^2 - \tilde{\eta}^2)/6$ (thick solid line) around the largest wave of WACSIS.

they tend to amplify wave envelopes symmetrically, as predicted by the NLS-type formulations (Socquet-Juglard et al. 2005; Mori and Janssen 2006, Gramstad and Trulsen 2007). Second-order corrections are introduced in the eventual solutions via the reconstruction formulae (cf. Socquet-Juglard 2005). All this, therefore, suggests that, if a wave record is rendered “nonskew” or vertically symmetric, then the resulting statistics should essentially reflect the effects of third-order quasi-resonant instabilities, if any.

To obtain a nonskew representation, say, $\tilde{\eta}$ of η , consider the second-order expression

$$\tilde{\eta} = \eta - \frac{\lambda_3}{6} (\eta^2 - \hat{\eta}^2). \quad (39)$$

The application of Eq. (39) in WACSIS, based on the half-hourly estimates of λ_3 in Fig. 2, gives $-0.014 \leq \langle \tilde{\eta}^3 \rangle \leq 0.027$ and $\langle \tilde{\eta}^3 \rangle = 0.008$ as an overall average as compared to $\lambda_3 = 0.231$ for η . The root mean square of $\tilde{\eta}$, wave height parameter r_m , and all joint cumulants of $\tilde{\eta}$ and its Hilbert transform remain practically the same as those of η and $\hat{\eta}$. However, $\mu = 0$ since $\tilde{\eta}$ is in essence “linearized.”

What the preceding analysis physically leads to is depicted in Fig. 24, showing short coincident segments of η , $\tilde{\eta}$, and the second-order correction $\lambda_3(\eta^2 - \hat{\eta}^2)/6$ removed from η to obtain $\tilde{\eta}$ around the largest wave of WACSIS. In Fig. 25 the distributions of zero upcrossing wave heights are compared as well as crest and trough

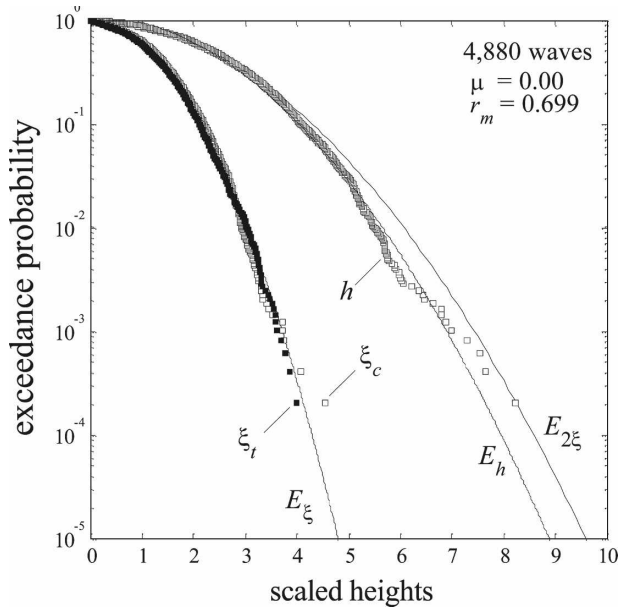


FIG. 25. Exceedance distributions of zero up-crossing wave heights (h), crest (ξ_c), and trough (ξ_t) amplitudes extracted from the nonskew series $\tilde{\eta}$ of WACSIS compared to E_h [Eq. (29)] for wave heights, $E_{2\xi}$ (Rayleigh ED) for narrowband wave heights ($h \cong 2\xi$), and E_ξ (Rayleigh ED) for linear crest and trough amplitudes.

amplitudes of $\tilde{\eta}$ with E_h from Eq. (29), $E_{2\xi}$ and E_ξ . Generally, second-order effects do not affect the statistics of the heights of oceanic waves significantly (Tayfun and Fedele 2007b). A comparison of Fig. 19 or Fig. 20 with Fig. 25 suggests that this is essentially so in WACSIS also. The observed heights are well represented by either E_h or $E_{2\xi}$ over larger waves, and the largest wave no longer appears so freakish as it does in Fig. 19. More significantly, E_ξ for linear waves now describes the crest and trough amplitudes in $\tilde{\eta}$ fairly well. These results indicate unequivocally that third-order modulational instabilities do not have any discernable relevance in WACSIS. So, the linearization procedure described above appears to offer a fairly effective and straightforward means of exploring if such instabilities do, in fact, affect the statistics of oceanic wind waves or not.

11. Conclusions

The validity of theoretical approximations developed for describing the joint, marginal, and conditional statistics of the envelope and phase of wind waves is confirmed by the WACSIS comparisons. The theoretical results suggest that wave phase statistics and the nature of surface displacements tend to differ appreciably but

predictably, depending on whether envelope elevations exceed the significant envelope height. For envelope elevations sufficiently larger than this threshold, wave phase distributions approach a simple limit form, indicating that large surface displacements can occur only above the mean sea level. This is likewise confirmed by the WACSIS data.

Larger waves appear more regular or narrow banded, and their heights and crests do not exceed the Miche–Stokes-type upper limits. This seems so even for unusually large waves often referred to as freak or rogue waves with scaled features and proportions similar to the largest wave captured by the WACSIS measurements. The random superposition of spectral components enhanced by the presence of second-order bound modes appears as the most likely mechanism that generates large surface displacements and thus such large waves under oceanic conditions.

Further analyses and the linearization of WACSIS all indicate that third-order NLS-type instabilities have no discernable effect on the surface statistics. Indeed, the nature of similar statistics observed in more extensive measurements representative of oceanic storm waves far more energetic than WACSIS is also entirely consistent with this conclusion (cf. Forristall 2000, 2007; Tayfun and Fedele 2007b). The largest wave in WACSIS would not have appeared so unusual had the measurements been maintained sufficiently longer or if many more wave probes had been deployed to gather an ensemble of simultaneous measurements. Because of the highly unstable nature of statistics associated with the largest observations, a sample population of about 5000 waves gathered at a fixed point in time may not always be adequate for reliably estimating the frequency of occurrence of the largest wave in a population.

Acknowledgments. The author is indebted to G. Z. Forristall, Ocean Engineering, Inc., Camden, ME, and M. Prevosto, Ifremer, for the WACSIS data, and to the reviewers for their constructive criticisms and useful insight.

APPENDIX A

Derivations of $p_{\xi^\pm}^\pm$ and $E_{\xi^\pm}^\pm$

Let $A^+ \equiv \{\eta > 0\} = \{|\phi| \leq \pi/2\}$ and $A^- \equiv \{\eta < 0\} = \{\pi/2 < |\phi| \leq \pi\}$. The conditional PDs $p_{\xi^+}^\pm$ and $p_{\xi^-}^\pm$, given A^+ and A^- , respectively, follow from probabilistic definitions as

$$p_{\xi^\pm}^\pm(z) \equiv \int_{A^\pm} p_{\phi\xi}(\phi, z) d\phi \Big/ \int_{A^\pm} p_\phi d\phi. \quad (A1)$$

Integrating Eq. (2) with respect to $\phi \in A^+$ for p_ξ^+ and $\phi \in A^-$ for p_ξ^- gives

$$\int_{A^\pm} p_{\phi\xi}(\phi, z) d\phi = \frac{p_\xi}{2} \left[1 \pm \frac{\lambda_3}{3\pi} z(z^2 - 4) \right], \quad (\text{A2})$$

where $p_\xi = z \exp(-z^2/2)$. And, from Eq. (6),

$$\int_{A^\pm} p_\phi d\phi \equiv P^\pm = \frac{1}{2} \left(1 \mp \frac{\lambda_3}{3\sqrt{2}\pi} \right), \quad (\text{A3})$$

as previously given in Eqs. (7) and (8). The substitution of the preceding results in (A1) leads to p_ξ^\pm in the form of Eq. (9). Integrating the latter over (z, ∞) gives the corresponding ED $\text{Pr}\{\xi^\pm > z\}$ as

$$E_\xi^\pm = \frac{E_\xi}{2P^\pm} \left\{ 1 \pm \frac{\lambda_3}{3\pi} \left[z^3 - z - \sqrt{\frac{\pi}{2}} \exp\left(\frac{z^2}{2}\right) \text{erfc}\left(\frac{z}{\sqrt{2}}\right) \right] \right\}, \quad (\text{A4})$$

where $E_\xi \equiv \text{Pr}\{\xi > z\} = \exp(-z^2/2)$. For $z \gg 1$, we can use the expansion

$$\sqrt{\frac{\pi}{2}} \exp\left(\frac{z^2}{2}\right) \text{erfc}\left(\frac{z}{\sqrt{2}}\right) = \frac{1}{z} \left(1 - \frac{1}{z^2} + \frac{3}{z^4} - \dots \right) \quad (\text{A5})$$

in (A4) to obtain Eq. (10) readily.

Numerical comparisons for $\lambda_3 < 0.3$ show that Eqs. (10) and (A4) are practically the same for $z > 1$, approximately. Further, $E^- < 0$ for $z > z^*$, where $z^*(z^{*2} - 1) \cong 3\pi/\lambda_3$, suggesting that negative minima less than $-z^*$ are not physically realizable. The comparison of E^- with the negative minima η_{\min} of WACIS in Fig. 8 seems consistent with this conjecture.

APPENDIX B

Expected Profile of Nonlinear Waves

Consider $\eta = \eta_1 + \eta_2$, where η_1 and η_2 , respectively, represent the linear first-order surface displacement and the second-order correction. Explicitly,

$$\eta_1(t) = \int \cos[\omega t + \varepsilon(\mathbf{k})] dZ(\mathbf{k}), \quad (\text{B1})$$

$$\eta_2(t) = \frac{1}{4} \iint [K^+ \cos\Phi^+ + K^- \cos\Phi^-] dZ(\mathbf{k}) dZ(\mathbf{k}') \quad (\text{B2})$$

in which $\varepsilon(\mathbf{k}) \equiv$ independent random phases distributed uniformly in $(0, 2\pi)$, $\mathbf{k} \equiv$ vector wavenumber with modulus k such that $\omega^2 = gk \tanh kd$, $d =$ water depth, $Z(\mathbf{k}) \equiv$ random spectral amplitudes with orthogonal increments, and $\langle |dZ|^2 \rangle = S(\mathbf{k}) d\mathbf{k}$; $S(\mathbf{k}) \equiv$ directional spectrum, $\Phi^\pm \equiv (\omega \pm \omega')t + \varepsilon(\mathbf{k}) \pm \varepsilon(\mathbf{k}')$, and $K^\pm = K^\pm(\mathbf{k}, \mathbf{k}')$ represent the interaction kernels associated with second-order bound waves (cf. Forristall 2000). On the assumption that η is zero mean and scaled with σ , the zero-order moment of S is unity. So, the skewness coefficient of η is given to the leading order by (cf. Tayfun 1994)

$$\lambda_3 = \langle \eta^3 \rangle = \frac{3}{2} \iint [K^+ + K^-] S(\mathbf{k}) S(\mathbf{k}') d\mathbf{k} d\mathbf{k}'. \quad (\text{B3})$$

Assume for the moment that second-order corrections are negligible, so that $\eta = \eta_1$, and $\eta_0 \equiv \eta(0) \gg 1$ represents a large wave crest. Then, the expected profile of $\eta(t)$, conditional on $\eta(0) \gg 1$, is given by (Lindgren 1972; Phillips et al. 1993; Boccotti 2000)

$$\langle \eta(t) | \eta_0 \gg 1 \rangle = \xi \rho(t) = \xi \int \cos(\omega t) S(\mathbf{k}) d\mathbf{k}, \quad (\text{B4})$$

where $\eta_0 \equiv \xi$ represents the Rayleigh-distributed wave crest, and ρ the normalized covariance kernel of η . Now, notice that (B4) follows from Eq. (B1), setting $\varepsilon = 0$ and $dZ = \xi S(\mathbf{k}) d\mathbf{k}$. Introducing the same substitutions in Eq. (B2) likewise leads to

$$\langle \eta_2(t) | \eta_0 \gg 1 \rangle = \frac{\xi^2}{4} \iint [K^+ \cos\beta^+ + K^- \cos\beta^-] S(\mathbf{k}) S(\mathbf{k}') d\mathbf{k} d\mathbf{k}', \quad (\text{B5})$$

where $\beta^\pm \equiv (\omega + \omega')t$ for brevity. Next, we substitute the kernel

$$\lambda(t) = \frac{3}{2} \iint [K^+ \cos\beta^+ + K^- \cos\beta^-] S(\mathbf{k}) S(\mathbf{k}') d\mathbf{k} d\mathbf{k}' \quad (\text{B6})$$

in Eq. (B5) and add the resulting expression to (B4) to obtain Eq. (27). A comparison of Eqs. (B3) and (B6) shows that $\lambda(t) \leq \lambda(0) = \lambda_3$, in general. Thus, setting $t = 0$ in Eq. (27) reduces it to Eq. (28).

Evidently, Eq. (27) satisfies the equations of wave motion to second order as a deterministic solution, just as $\eta = \eta_1 + \eta_2$ does as a random solution, in general.

Further, the extension of the preceding results to the expected structure of η as a three-dimensional surface simply requires that ρ and λ be defined more generally as functions of both temporal and spatial variables in a manner consistent with the random spectral representations of η_1 and η_2 in the most general case.

REFERENCES

- Al-Humoud, J., M. A. Tayfun, and H. Askar, 2002: Distribution of nonlinear wave crests. *Ocean Eng.*, **29**, 1929–1943.
- Boccotti, P., 2000: *Wave Mechanics for Ocean Engineering*. Elsevier Science, 405 pp.
- Cartwright, D. E., and M. S. Longuet-Higgins, 1956: The statistical distribution of the maxima of a random function. *Proc. Roy. Soc. London*, **237A**, 212–232.
- Cherneva, Z., and C. Guedes Soares, 2006: Estimation of the bispectra and phase distribution of storm sea states with abnormal waves. *Ocean Eng.*, **34**, 2009–2020.
- , P. Petrova, N. Andreeva, and C. Guedes Soares, 2005: Probability distributions of peaks, troughs and heights of wind waves measured in the Black Sea coastal zone. *Coastal Eng.*, **52**, 599–615.
- Dysthe, K., K. Trulsen, H. Krogstad, and H. Socquet-Juglard, 2003: Evolution of a narrow-band spectrum of random surface gravity waves. *J. Fluid Mech.*, **478**, 1–10.
- Fedele, F., 2008: Rogue waves in oceanic turbulence. *Physica D*, **237**, 2127–2131.
- Forristall, G. Z., 2000: Wave crest distributions: Observations and second-order theory. *J. Phys. Oceanogr.*, **30**, 1931–1943.
- , 2007: Comparing hindcasts with measurements from Hurricanes Lili, Ivan, and Katrina. *Proc. 10th Int. Workshop on Wave Hindcasting and Forecasting*, Oahu, HI, 20 pp. [Available online at www.waveworkshop.org/10thWaves/ProgramFrameset.htm.]
- , H. E. Krogstad, P. H. Taylor, S. S. Barstow, M. Prevosto, and P. Tromans, 2002: Wave crest sensor intercomparison study: An overview of WACSYS. *Proc. 24th Int. Conf. on Offshore Mechanics and Arctic Engineering*, OMAE2002-28438, Oslo, Norway, American Society of Mechanical Engineers, 11 pp.
- Goda, Y., 1978: The observed distribution of periods and heights of sea waves. *Proc. 16th Int. Conf. on Coastal Engineering*, Hamburg, Germany, American Society of Civil Engineers, 227–246.
- Gramstad, O., and K. Trulsen, 2007: Influence of crest and group length on the occurrence of freak waves. *J. Fluid Mech.*, **582**, 463–472.
- Lindgren, G., 1972: Local maxima of Gaussian fields. *Arkiv Matematik*, **10**, 195–218.
- Longuet-Higgins, M. S., 1957: The statistical analysis of a random moving surface. *Philos. Trans. Roy. Soc. London*, **966A**, 321–387.
- , 1963: The effect of nonlinearities on statistical distributions in the theory of sea waves. *J. Fluid Mech.*, **17**, 459–480.
- , 1975: On the joint distribution of the periods and amplitudes of sea waves. *J. Geophys. Res.*, **80**, 2688–2694.
- Miche, R., 1944: Mouvements ondulatoires de la mer en profondeur constante ou décroissante (in French). *Ann. des Ponts et Chaussées*, **121**, 285–318.
- Mori, M., M. Onorato, P. A. E. M. Janssen, A. R. Osborne, and M. Serio, 2007: On the extreme statistics of long-crested deep water waves: Theory and experiments. *J. Geophys. Res.*, **112**, C09011, doi:10.1029/2006JC004024.
- Mori, N., and P. A. E. M. Janssen, 2006: On kurtosis and occurrence probability of freak waves. *J. Phys. Oceanogr.*, **36**, 1471–1483.
- Onorato, M., A. R. Osborne, M. Serio, L. Cavaleri, C. Brandini, and C. T. Stansberg, 2006: Extreme waves, modulational instability and second order theory: Wave flume experiments on irregular waves. *Euro. J. Mech. B*, **25**, 583–601.
- Phillips, O. M., D. Gu, and M. Donelan, 1993: Expected structure of extreme waves in a Gaussian sea. Part I: Theory and SWADE buoy measurements. *J. Phys. Oceanogr.*, **23**, 992–1000.
- Rodriguez, G., C. Guedes Soares, E. P. Martell, and J. C. Nieto, 1998: Non-uniformity in the wind-generated gravity waves phase distribution. *Proc. 26th Int. Conf. on Coastal Engineering*, Copenhagen, Denmark, American Society of Civil Engineers, 3668–3679.
- Socquet-Juglard, H., 2005: Spectral evolution and probability distributions of surface ocean gravity waves and extreme events. D.Sc. thesis, Department of Mathematics, University of Bergen, 65 pp.
- , K. Dysthe, K. Trulsen, H. E. Krogstad, and J. D. Liu, 2005: Probability distributions of surface gravity waves during spectral changes. *J. Fluid Mech.*, **542**, 195–216.
- Tayfun, M. A., 1994: Distributions of wave envelope and phase in weakly nonlinear random waves. *J. Eng. Mech.*, **120**, 1009–1025.
- , 2006: Statistics of nonlinear wave crests and groups. *Ocean Eng.*, **33**, 1589–1622.
- , and J.-M. Lo, 1989: Envelope, phase and narrow-band models of sea waves. *J. Waterway Port Coastal Ocean Eng.*, **115**, 594–613.
- , and —, 1990: Non-linear effects on wave envelope and phase. *J. Waterway Port Coastal Ocean Eng.*, **116**, 79–100.
- , and F. Fedele, 2007a: Expected shape of large waves in storm seas. *Proc. 26th Int. Conf. on Offshore Mechanics Arctic Engineering*, San Diego, CA, American Society of Mechanical Engineers, OMAE2007-29073, 8 pp.
- , and —, 2007b: Wave-height distributions and nonlinear effects. *Ocean Eng.*, **34**, 1631–1649.
- Tulin, M. P., and J. J. Li, 1992: On the breaking of energetic waves. *Int. J. Offshore Polar Eng.*, **2**, 46–53.